Exotic Inverse Kinetic Isotopic Effect in the Thermal Decomposition of Levitated Aluminum Iodate Hexahydrate Particles

Grace L. Rizzo, Souvick Biswas, Ivan Antonov, Kelsea K. Miller, Michelle L. Pantoya,* and Ralf I. Kaiser*

Read Online

ACCESS | Metrics & More | Article Recommendations | Supporting Information

ABSTRACT: Aluminum iodate hexahydrate ($[Al(H_2O)_6](IO_3)_3(HIO_3)_2$; AIH) represents a novel, oxidizing material for energetic applications. Recently, AIH was synthesized to replace the aluminum oxide passivation layer of aluminum nanoenergetic materials (ALNEM). The design of reactive coatings for ALNEM-doped hydrocarbon fuels in propulsion systems requires fundamental insights of the elementary steps of the decomposition of AIH. Here, through the levitation of single AIH particles in an ultrasonic field, we reveal a three-stage decomposition mechanism initiated by loss of water (H_2O) accompanied by an unconventional inverse isotopic effect and ultimate breakdown of AIH into gaseous elements (iodine and oxygen). Hence, AIH coating on aluminum nanoparticles replacing the oxide layer would provide a critical supply of oxygen in direct contact with the metal surface thus enhancing reactivity and reducing ignition delays, further eliminating decades-old obstacles of passivation layers on nanoenergetic materials. These findings demonstrate the potential of AIH to aid in the development of next-generation propulsion systems.
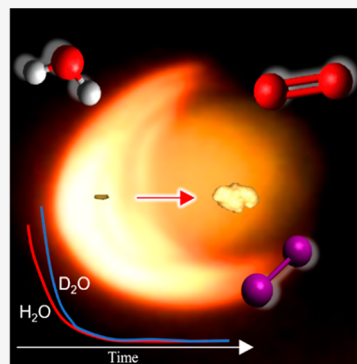
Ever since the discovery of *Ruby Gold* (colloidal suspensions of gold nanoparticles) more than 150 years ago by Michael Faraday,[1] metallic nanostructures have emerged as attractive high-energy-density materials.[2] With a volumetric energy density of 84 kJ cm^{-3},[3] particular attention has been devoted to the synthesis of aluminum nanoenergetic materials (ALNEMs) as additives to hydrocarbon fuels such as exo-tetrahydrodicyclopentadiene ($C_{10}H_{16}$, JP-10) in air-breathing propulsion systems.[4,5] These nanoparticles exceed the limited volumetric energy densities of traditional hydrocarbons (35−40 kJ cm^{-3}). However, the exploitation of ALNEMs in combustion systems revealed vital limitations in the form of an inert layer of aluminum oxide (Al_2O_3) on the surface.[6−8] This oxide layer significantly reduces the rate of reaction with the passivation layer not only acting as a heat sink but also limiting the diffusion of oxygen and hence the combustion of the aluminum core.[6−8] Therefore, the replacement of the aluminum oxide passivation layer with reactive coatings, which allow a rapid supply of oxygen to the aluminum nanoparticle and hence an increase in reactivity, would represent an attractive approach to eliminate the long-standing obstacles of the passivation layers.[9−12]

Aluminum iodate hexahydrate ($[Al(H_2O)_6](IO_3)_3(HIO_3)_2$; AIH) has attracted substantial attention for the replacement of the aluminum oxide layer considering its low oxygen release temperatures and potential in forming highly reactive oxidizer gases including oxygen (O_2) and iodine (I_2) during its decomposition.[9−12] Preliminary studies exploiting AIH-doped explosives such as trinitrotoluene (TNT) revealed a 30% increase in detonation velocity;[13] this allowed the particles to react on time scales equivalent to the detonation event, hence ultimately enhancing the energy release rate in aluminum nanoparticles.[14,15] However, although AIH represents a promising coating on aluminum nanoparticles, there is still a critical lack of fundamental knowledge of the underlying mechanisms of distinct stages in the thermal decomposition of pure AIH. This understanding is vital to the development of next-generation, metal nanoparticle-based propulsion systems along with energy-generation technologies and requires the systematic identification of key reaction intermediates along with the underlying reaction mechanisms and decomposition kinetics.

Here, exploiting ultrasonic levitation technology, three distinct stages were exposed in the thermal decomposition of single, levitated AIH and AID particles in an argon inert atmosphere: a rapid loss of water (H_2O) along with a volume increase of the levitated particle by 200% commencing at 375 ± 5 K, the slow conversion of iodic acid (HIO_3) into diiodine pentoxide (I_2O_5) and water (H_2O) starting at 480 ± 5 K, and a rapid decomposition of diiodine pentoxide accompanied by vigorous gas release into its elements (iodine and oxygen) beginning at 580 ± 5 K with onset decomposition temperatures significantly *lower* for singly levitated particles than reported for bulk AIH by up to 82 K.

(a)

(b)
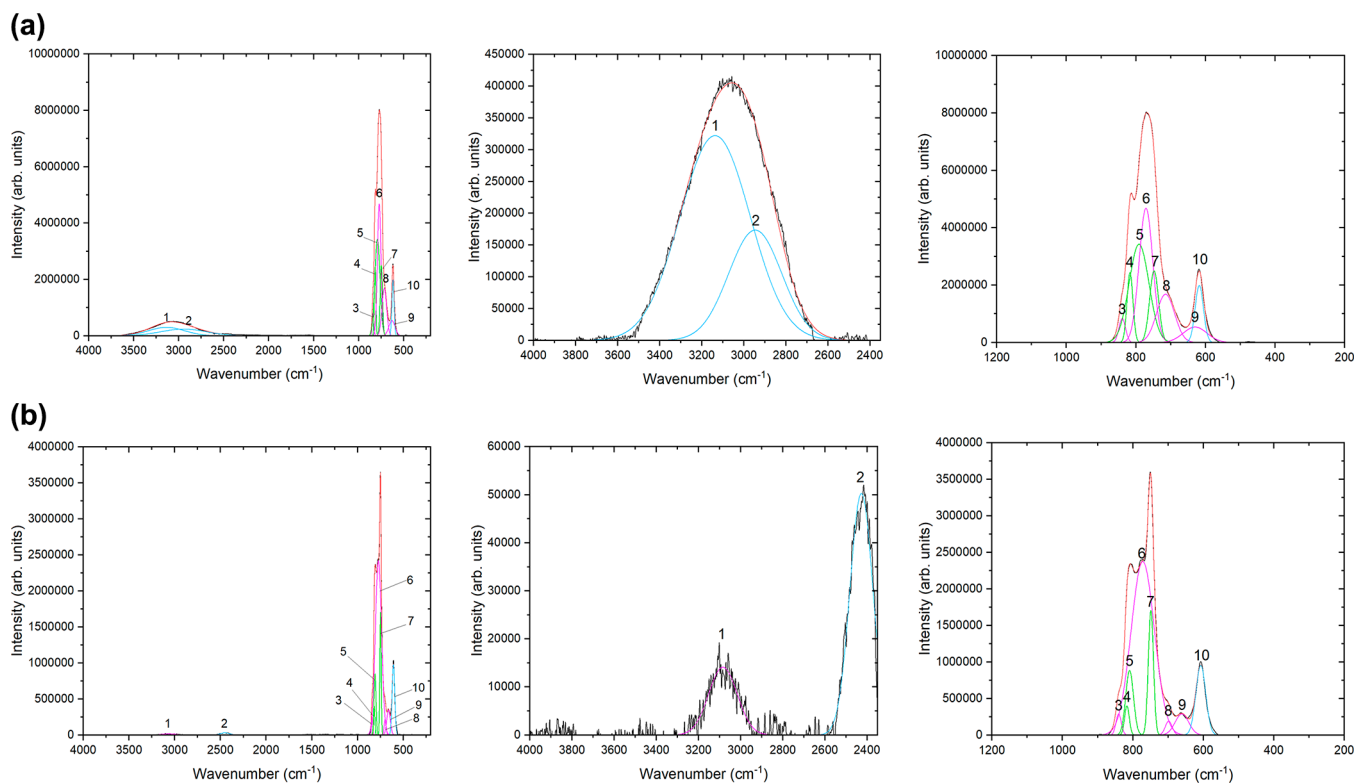
Figure 1. Raman Spectra of (a) AIH and (b) AID at 298 K. The far left panel is the full deconvoluted spectrum from 4000 to 200 cm^{-1}; the middle panel represents the high region peaks from 4000 to 2350 cm^{-1}; the far right panel is the deconvoluted peaks in the low region from 1200 to 200 cm^{-1}. The spectrum (black) is deconvoluted to make a peak fitted spectrum (red). Deconvoluted peaks are assigned to water (blue), iodic acid (pink), and iodate ion (green). See Table S1a,b for peak assignments.

(a)

(b)
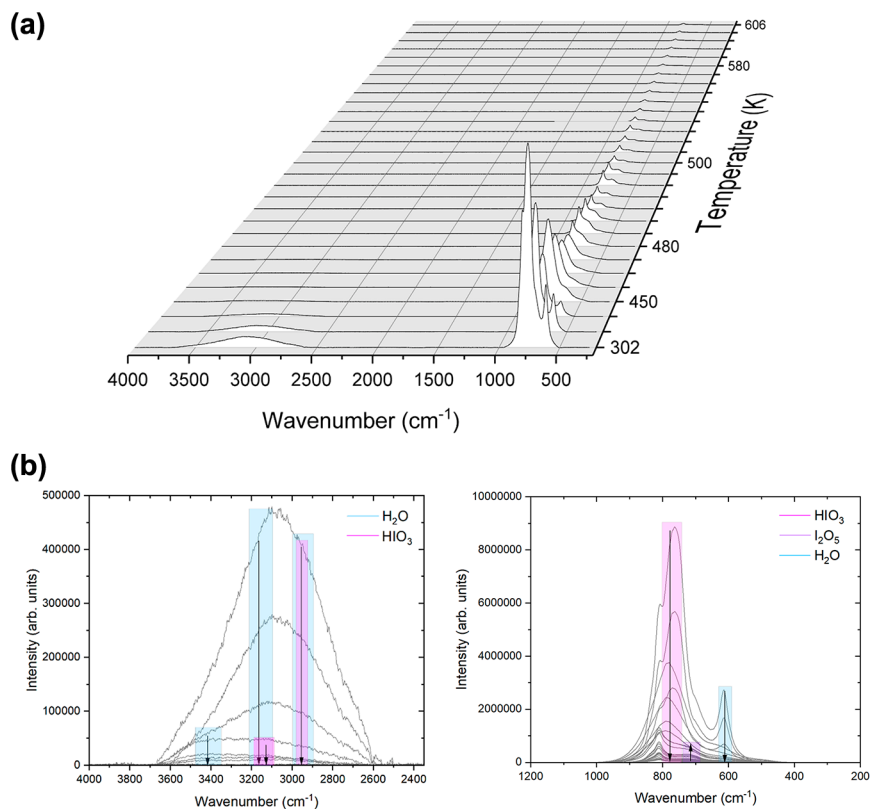
Figure 2. (a) 3D plot of the Raman spectra of AIH from 302 to 606 K. (b) High and low regions of the spectra taken in panel a. Arrows indicate the decrease and increase of the species H_2O (blue), HIO_3 (pink), and I_2O_5 (purple).

Table 1. Vibrational Mode Assignments for the Observed Peaks in the Raman Spectra of AIH and AID after Heating beyond 480 K

peaks	frequency (cm⁻¹) (this work)	intensity (this work)	frequency (cm⁻¹) (literature[17,20−22,24])	literature intensity	carrier	assignment	description
				AIH			
4	813	m	817	vw	IO_3^-	combination	combination
5	808	s	808, 806, 789	s	IO_3^-	ν_3	IO₂ antisymmetric stretching
		m	810	vs	I_2O_5	ν_s	O−I=O stretch
a	726	m	724	s	I_2O_5		O−I=O stretch
b	613	m	607	m	I_2O_5		IO stretch
c	533	w	535	vw	I_2O_5		combination
				AID			
4	814	m	817	vw	IO_3^-	combination	combination
5	806	s	808, 806, 789	s	IO_3^-	ν_3	IO₂ antisymmetric stretching
		m	810	vs	I_2O_5	ν_s	O−I=O stretch
a	728	m	724	s	I_2O_5		O−I=O stretch
b	627	m	607	m	I_2O_5		IO stretch
c	501	w	535	vw	I_2O_5		combination

Against conventional wisdom, these studies also afford persuasive testimony on an *inverse isotope effect* for the loss of deuterated water versus water in levitated AID and AIH particles with $k_1(D_2O)/k_1(H_2O) = 5.3 \pm 0.6$ at 375 ± 5 K. A potential rationale for this *inverse isotopic effect* is the red-shift of the vibration modes to lower energies for deuterated water, predominantly for the symmetric and antisymmetric stretching modes from 3531 to 2659 cm⁻¹ (AIH) and 2659 cm⁻¹ to 2000 cm⁻¹ (AID) ranges, thus increasing the energy absorption of deuterated water compared to normal water and enhancing the rate of D₂-water loss compared to normal water. Overall, the fundamental knowledge obtained here reveals that AIH used as an aluminum nanoparticle coating would not only replace the aluminum oxide layers but also augment the thrust through the development of gaseous decomposition products in propulsion systems (H_2O, I_2, and O_2) with molecular oxygen released throughout the decomposition of diiodine pentoxide, supplying an extra source of an oxidizer directly in contact with the surface of the aluminum nanoparticles, possibly reducing ignition delays, and ultimately improving proficiency of propulsion systems.

Raman spectroscopy represents an outstanding methodology to trace the decomposition of levitated AIH/AID particles in an inert atmosphere of argon and to identify new molecules formed in these processes. This requires first an assignment of the peaks in the nonprocessed AIH/AID samples at 293 K with the deconvoluted Raman spectra depicted in Figure 1; the resulting peaks were compared with literature data and are compiled in Table S1 for AIH and AID.[16−22]

In the high-wavenumber region covering 3600 to 2600 cm⁻¹, the most intense features correspond to the antisymmetric and symmetric OH stretching modes of the water (H_2O) ligands coordinating the aluminum cation center, i.e., ν_3 (3137 cm⁻¹; peak 1) and ν_1 (2946 cm⁻¹; peak 2). Note that contributions to the latter feature can also originate from the symmetric stretching of the OH moiety in iodic acid (HIO_3). In the low-wavenumber region from 900 to 500 cm⁻¹, four features linked to iodic acid (HIO_3) are noticeable: $\nu_8 + \nu_L$ (834 cm⁻¹; peak 3), ν_8 (777 cm⁻¹; peak 6), ν_3 (713 cm⁻¹; peak 8), and ν_4 (631 cm⁻¹; peak 9). The $\nu_8 + \nu_L$ features are characterized as a combination of the IO₂ antisymmetric stretch (ν_8) and a libration mode; ν_3 and ν_4 correspond to IO₂ symmetric stretching mode and IO

stretch, respectively. Along with these bands, three bands from the iodate anion (IO_3^-) are visible: a combination band, the IO₂ antisymmetric stretch (ν_3), and the IO₂ symmetric stretch (ν_1) positioned at 816 cm⁻¹ (peak 4), 790 cm⁻¹ (peak 5), and 752 cm⁻¹ (peak 7), respectively. Finally, the peak at 618 cm⁻¹ (peak 10) could be associated with the lattice and/or vibration mode (ν_L) of $[Al(H_2O)_6]^{3+}$. If we compare the spectrum for AID, we find in the high-wavenumber region the same ν_1 symmetric stretching of HIO_3 (3084 cm⁻¹; peak 1) as seen in AIH. Along with this feature, the OD bending mode is red-shifted compared to AIH and identified for the D₂O ligand ($2 \times \delta(OD_2)$) at 2427 cm⁻¹ (peak 2). For the low-wavenumber region, all bands hold essentially the same assignments as for AIH shifted by between 5 and 30 cm⁻¹.

Having benchmarked the Raman spectra of the neat AIH and AID samples, the inherent changes of the Raman spectra upon heating with a carbon dioxide (CO_2) laser from 302 K until the particles detrap at about 606 K are explored (Figure 2 and Table 1).

As the temperature of the heated AIH particles approached 375 K, the features attributed to water (3137, 2946, and 618 cm⁻¹) began to decrease (Figure 2a). This finding can be recognized as a loss of water from the hexacoordinated aluminum ion to the gas phase (eq 1). Once the temperature reached 450 K, a sudden rise in the intensity of the peaks associated with iodic acid (777, 713, and 631 cm⁻¹) was noticed; upon further increasing the temperature, at 480 K these features started to decline. Simultaneously, a rise in intensity of diiodine pentoxide (I_2O_5) features centered at 726, 613, and 533 cm⁻¹ was clearly visible. These observations reveal the decomposition of iodic acid (HIO_3) to diiodine pentoxide (I_2O_5) plus water (H_2O) (eq 2). Above 580 K, the diiodine pentoxide peaks begin to decline, suggesting thermal decomposition of diiodine pentoxide (I_2O_5) into iodine (I_2) and oxygen (O_2) (eq 3).

$$[Al(H_2O)_6](IO_3)_3(HIO_3)_2 \rightarrow Al(IO_3)_3(HIO_3)_2 + 6H_2O \tag{1}$$

$$Al(IO_3)_3(HIO_3)_2 \rightarrow Al(IO_3)_3 + I_2O_5 + H_2O \tag{2}$$

$$I_2O_5 \rightarrow I_2 + \frac{5}{2}O_2 \tag{3}$$
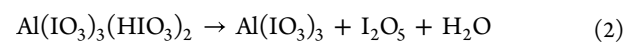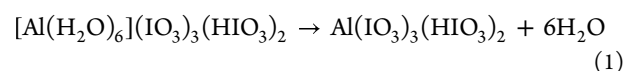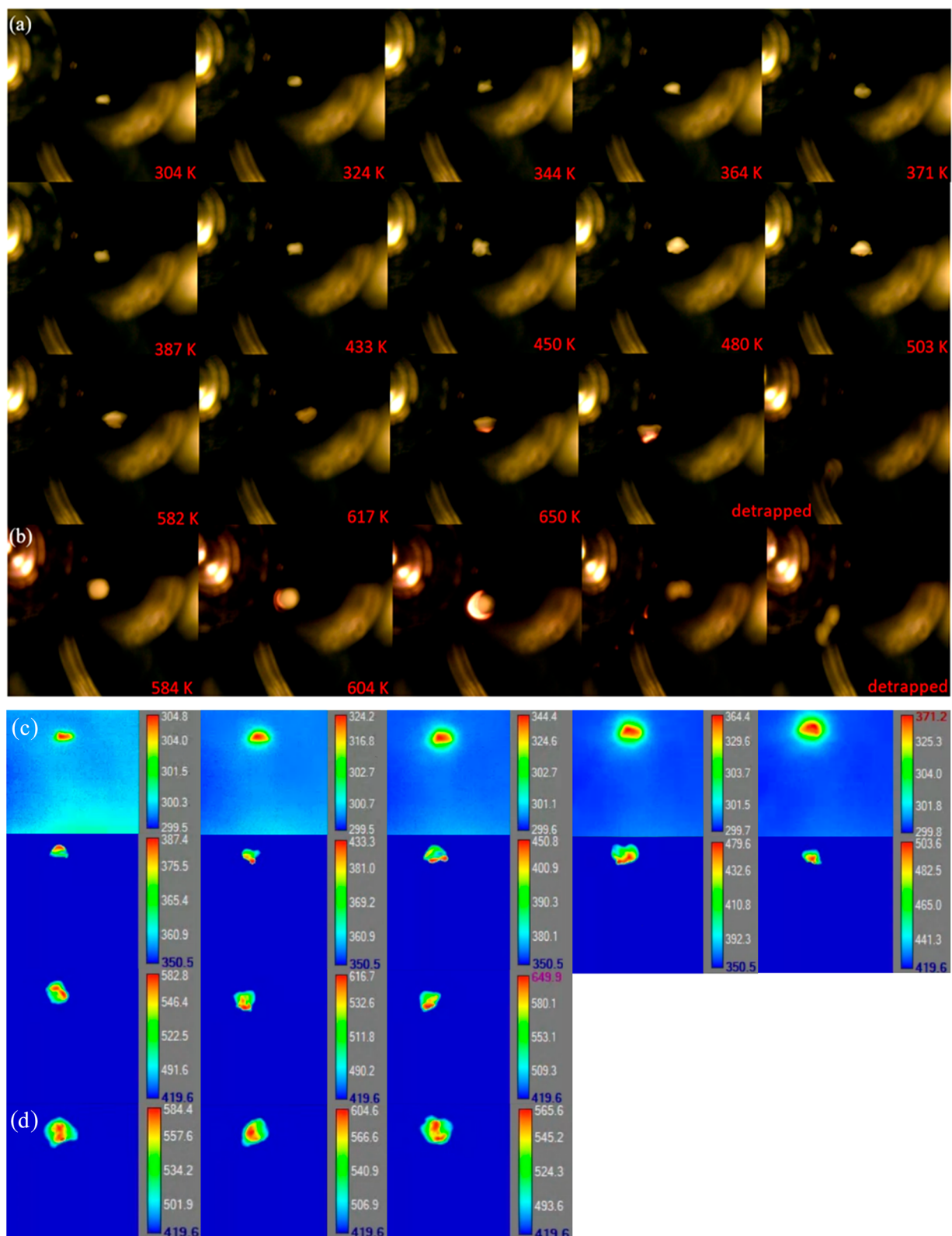
Figure 3. (a and b) Optical images of two different levitated AIH particles, at varying temperatures. Particle a was heated to a max temperature of 650 K where it detrapped soon after reaching 650 K. The appearance of red smoke was observed around 580 K. Flames appeared past 600 K. Particle b showed flame starting at 604 K. The two frames after 604 K were observed to show intense flames with an ejection of a small particle soon after. (c and d) Corresponding infrared images of the two different levitated AIH particles from panels a and b. Infrared images were taken in units of Kelvin.

Simultaneously with the Raman study, high-speed optical videos and infrared images were collected to observe changes as the particles approached the temperatures of 375 ± 5, 480 ± 5, and 580 ± 5 K, where significant alterations were observable in the Raman spectra (Supporting Information; Movies M1−M8).
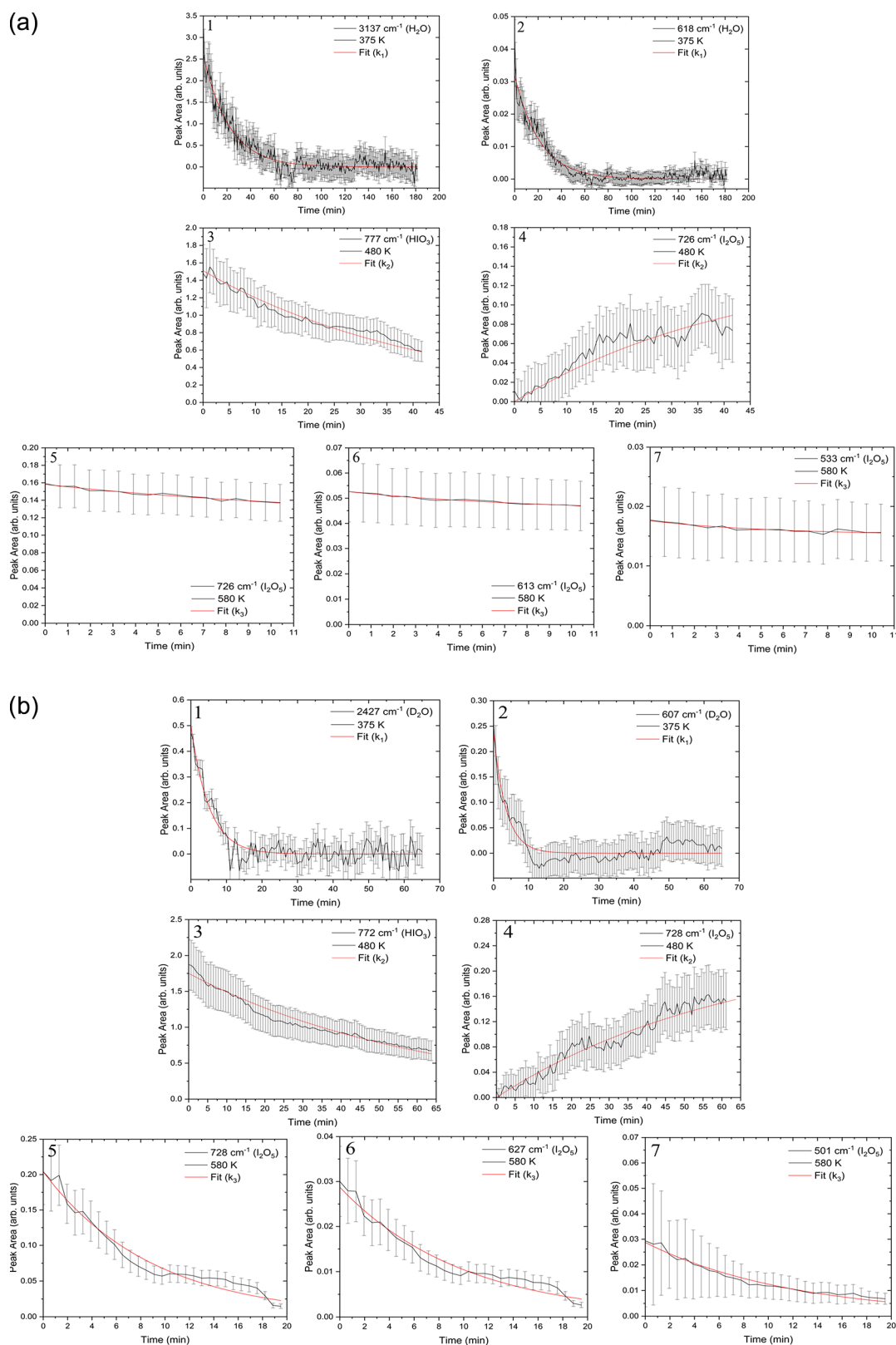
Figure 4. Fitted time traces of selected bands in the Raman spectra for (a) AIH and (b) AID at each step in the heating process. The component/species are also mentioned in the parentheses of the corresponding band positions. See Tables S2 and S3 for rate constants.

Critical snapshots are displayed in Figure 3 for the AIH system for two particles (a) (M1-M6) and (b) (M7, M8).

As the heating commences to 371 ± 5K (Figure 3a), the AIH particles slowly increase in volume by about 20%; upon reaching

371 ± 5 K, a "popcorning" effect was visible, supported by a rapid enhancement of the particle volume by nearly 200% of its original size. As the temperature increases further, at 387 ± 5 K, a maximum volume increase of about 600% was observed. This

phase of the volume expansion corresponds to the spectroscopically detected loss of water molecules from the coordination sphere of the aluminum ions into the gas phase. The persistent temperature increase to 450 ± 5 K was accompanied by an increase in reflectivity of the surface of the levitated particle. Recall that at 450 ± 5 K, the Raman features of iodic acid (HIO_3) also rose in intensity. We may therefore conclude that iodic acid diffused from the inner AIH particle to the surface. Starting at about 480 ± 5 K, the temperature when iodic acid decomposed to diiodine pentoxide (I_2O_5) and water (H_2O), the particle started to decrease in volume by about 20%, and the surface darkened. As the temperature increased further, the surfaces of both particles became darker and released reddish-purple vapor; this phase was accompanied by a reduction in volume by about 50% at 582 ± 5 K. Considering eq 3, these reddish-purple vapors are associated with iodine released from the particles. Considering the balanced chemical equation, this process also releases molecular oxygen. As a result, both particles self-ignited, producing flames followed by rapid detrapment of the particles at temperatures exceeding 600 ± 5 K. Recall that the thermal decomposition was conducted in an argon inert atmosphere. Therefore, the ignition of the AIH particle is the result of the enhanced concentration of oxygen released from the levitated particle, which allows the particle to ignite and burn.

The aforementioned studies provide compelling evidence on a three-step process of the decomposition of AIH and AID: the loss of water at T1 = 375 ± 5 K (eq 1), the conversion of iodic acid into diiodine pentoxide and water at T2 = 480 ± 5 K (eq 2), and the decomposition of diiodine pentoxide into its elements (iodine and oxygen) starting at T3 = 580 ± 5 K. Vital quantitative information on the decomposition process can be gained by extracting time profiles of key species in the decomposition process (water, iodic acid, and diiodine pentoxide), which in turn can be fit kinetically to report rate constants. To provide this information, Raman spectra were collected at three distinct temperatures (T1, T2, and T3) over time for AIH and AID. These spectra were then deconvoluted, and the peak areas were integrated and plotted over time (Supporting Information, Figures S1−S7).

At a constant temperature of 375 ± 5 K, the collected Raman spectra were deconvoluted for both the levitated AIH and AID particles exploiting a Python code (see Supporting Information S1 and S2). The temporal evolution of the water features in AIH are displayed in Figure 4a (1 and 2) for 3137 and 618 cm^{-1}; the decay of the D$_2$-water peaks in the AID sample are traced in Figure 4b (1 and 2) at 2427 and 607 cm^{-1}. Both the water and D$_2$-water losses could be formally fit with a unimolecular decay (first-order reaction) following eq 4 with $[A]_t$ representing the concentration of reactant A at time t expressed via the peak area, $[A]_0$ is the initial concentration expressed via the peak area, k_1 the rate constant at 375 K, and t the time.[23] Laser fluctuations and particle movements account for the errors of the traces.

$$[A]_t = [A]_0 e^{-k_1 t} \tag{4}$$

This strategy provides a first-order rate constant of 0.047 ± 0.001 min^{-1} for AIH averaged over both traces (Tables S2 and S3). However, for the AID system, a first-order rate constant of 0.24 ± 0.02 min^{-1} was determined. This suggests that the loss of D$_2$-water proceeds faster than the loss of water revealing an *inverse* isotope effect with $k_1(D_2O)/k_1(H_2O) = 5.3 \pm 0.6$ for T1 = 375 ± 5 K.

For a constant temperature of 480 ± 5 K, the traces of the decay of iodic acid (HIO_3; 777 cm^{-1}, 772 cm^{-1}) and the emergence of diiodine pentoxide (I_2O_5; 726 cm^{-1}, 728 cm^{-1})[17,20−22,24] are displayed in Figure 4a (3 and 4) and Figure 4b (3 and 4) for AIH and AID, respectively. Fits were achieved by formally treating iodic acid as a dimer ($(HIO_3)_2$). $[A]_t$ follows a pseudo-first order reaction (eq 5); fits for the diiodine pentoxide product follow eq 6 with $[B]_t$ being the concentration of product B at time t.[23] For both the AIH and AID system, the rate of reaction, k_2, was found to be identical, i.e. $k_2 = 0.020 \pm 0.001$ min^{-1}. Hence, no isotope effect is observable. Note that the rate constant k_2 is about half of k_1, revealing a faster dehydration of water in the coordination sphere of the aluminum ion (eq 1) than the condensation reaction of two iodic acid molecules to diiodine pentoxide plus water (eq 2).

$$[A]_t = [A]_0 e^{-k_2 t} \tag{5}$$

$$[B]_t = [A]_0 (1 - e^{-k_2 t}) \tag{6}$$

For a constant temperature of 580 ± 5 K, the decomposition of diiodine pentoxide (eq 3) was monitored via the first-order decay (k_3) in the AIH and AID systems through the features at 726, 613, and 533 cm^{-1} (AIH) and 728, 627, and 501 cm^{-1} (AID). The rate constants, k_3, were determined to be 0.125 ± 0.051 min^{-1} and 0.099 ± 0.004 min^{-1} for AIH and AID, respectively, i.e., identical rates within the error limits. The absence of isotope effects in steps II and III is reflected in the fact that no deuterated reactants were involved in the decomposition processes. Note that phase III is accompanied by a facile detrapment of the particle considering the release of the gases and self-ignition. However, we were also able to extract kinetic traces for the AIH system at 600 ± 5 K yielding a rate constant of 1.01 ± 0.07 min^{-1} (Table S2 and Figure S8), i.e., a $810 \pm 380\%$ enhancement of the reaction rate by increasing the temperature by only about 3%, i.e., 20 ± 10 K. Following the Arrhenius law,[23] this translates into a classical activation energy of 303 ± 180 kJ mol^{-1} for the decomposition of diiodine pentoxide to its elements via eq 3 being endothermic by 173 kJ mol^{-1} at 298 K.

In conclusion, the decomposition of single, levitated AIH and AID particles in an argon inert atmosphere involves three discrete stages: the loss of water (H_2O) commencing at 375 ± 5 K (phase I), the conversion of iodic acid (HIO_3) into diiodine pentoxide (I_2O_5) and water (H_2O) starting at 480 ± 5 K (phase II), and the decomposition of diiodine pentoxide into the elements (iodine and oxygen) beginning at 580 ± 5 K (phase III). Most critically, for phase I and III, the decomposition onset temperatures are significantly *lower* for singly levitated particles than those reported for bulk AIH exploiting differential scanning calorimetry by up to 82 K.[10] This discovery stipulates conducting decomposition studies with single particles, i.e., the real conditions under which the additives are injected into combustion systems, to obtain precise onsets of decomposition, which might otherwise be masked by the bulk material. These studies provide compelling evidence on an *inverse isotope effect* for the loss of deuterated water versus water in levitated AID and AIH particles with $k_1(D_2O)/k_1(H_2O) = 5.3 \pm 0.6$ at 375 ± 5 K. Our findings of an *inverse isotopic effect* would gain support from previous dehydration studies of mono- and hexa-hydrated main group II (M = Ca^{2+}, Sr^{2+}) iodates $[M(D_2O)(IO_3)_2]$ versus $[M(H_2O)(IO_3)_2]$ and $[M(D_2O)_6(IO_3)_2]$ versus $[M(H_2O)_6(IO_3)_2]$ exploiting thermogravimetric (TG) and differential thermal analysis (TGA); these works report temperatures of D$_2$-water losses lower by 10 to 20 K compared to normal

water with averaged dehydration enthalpies of 115 versus 93 kJ mol^{-1}.[25−27] The *inverse isotopic effect* observed for AIH versus AID operates against conventional wisdom that due to the heavier mass of deuterium versus hydrogen, heavier isotopologues have lower vibrational frequencies compared to their lighter counterparts. This in turn would require a greater energy input for heavier isotopologues to overcome the transition state of a chemical reaction, thus reducing the rate constants;[23] this was observed, e.g., in catalytic reactions,[28] and in the combustion of metallic and organic energetic materials of, e.g., nanoaluminum with water,[29] and octahydro-1,3,5,7-tetranitro-1,3,5,7-tetrazocine (HMX);[30] these normal kinetic isotope effects evidenced the critical role of a kinetically controlled combustion process. The *inverse isotopic effect* of the dehydration of AIH versus AID here is challenging to reconcile with formerly postulated diffusion-limited dehydration steps of minerals with water in the coordination sphere of metal ions,[27] which should cause a *normal kinetic isotope effect* with the dehydration being faster for water compared to deuterated water. A promising rationalization for the *inverse isotopic effect* is the red-shift of the vibration modes to lower energies for deuterated water, predominantly the symmetric and antisymmetric stretching modes covering the 3531−2659 cm^{-1} (AIH) and 2659−2000 cm^{-1} (AID) ranges (Figure 5).
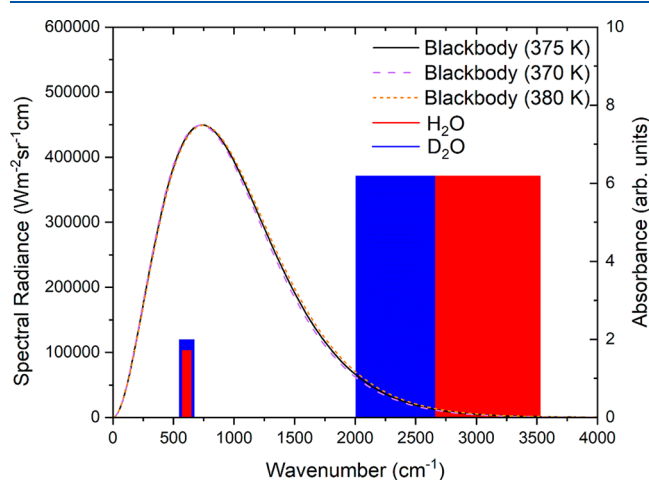
Figure 5. Blackbody spectra for 370, 375, and 380 K. The blackbody spectra are overlaid with the vibrational modes of water (H_2O) and deuterated water (D_2O). Relative absorbances of the water bands (3137, 2946, and 618 cm^{-1}) and deuterated water (2427 and 607 cm^{-1}) are shown.

Since these regions reveal a significantly enhanced overlap with the blackbody emission spectrum of the particles at 375 ± 5 K, this could result in an enhanced energy absorption of deuterated water compared to normal water.[31] This in turn would lead to a boosted loss of deuterated water compared to water due to the increased energy absorption and higher rate to overcome the transition state of the reaction.

The fundamental knowledge obtained from the decomposition studies of singly levitated AIH and AID particles along with the observation of an inverse isotopic effect provide quantitative insights into discrete stages, onsets of decompositions, intermediates (I_2O_5), and gases formed (H_2O, I_2, O_2) covering temperatures up to about 600 K. Therefore, AIH as a coating of aluminum nanoparticles would not only replace the oxide layers[9,10,12,32] but also amplify the thrust through the

development of gaseous decomposition products in propulsion systems. The molecular oxygen released via the decomposition of diiodine pentoxide also provides an additional source of an oxidizer which, in direct contact with the surface of the aluminum nanoparticles, could potentially reduce ignition delays, thus enhancing the efficiency of propulsion systems. Further, the iodine gas produced neutralizes bacteria and ultimately sterilizes potentially biologically contaminated environments including engine systems.[33]

Overall, these results represent a very first step to a systematic understanding of the decomposition processes of energetic coatings such as AIH on metal nanoparticles ultimately aiding in the development of next-generation, metal nanoparticle-based propulsion systems along with energy-generation technologies exploiting AIH-coated aluminum nanoparticles. This work further provides an experimental benchmark for prospective high-level computational investigation of the decomposition of AIH and AID in the condensed phase, in particular the inverse isotope effect as observed here, which is currently beyond reach. From the experimental aspect, ignition studies of single levitated JP-10 fuel droplets doped with AIH-coated aluminum nanoparticles are highly desirable to explore the impact of the AIH coating on the combustion stages of JP-10 and ignition delays ultimately augmenting the proficiency of propulsion systems.[34]

■ ASSOCIATED CONTENT

ⓢ Supporting Information

The Supporting Information is available free of charge at https://pubs.acs.org/doi/10.1021/acs.jpclett.3c00273.

> Details of the materials and methods used in experimentation; Raman vibrational assignments for AIH and AID at 293 K; AIH Raman spectra at 375, 480, 580, and 600 K; AID Raman spectra at 375, 480, and 580 K; time traces of AIH at 600 K; AIH and AID rate constants; Python script; levitator diagram; and pulse sequence (PDF)

> Movie M1, particle 1 size increase seen at 375 K; Movie M2, corresponding IR video for particle 1 at 375 K; Movie M3, particle 1 view at 480 K; Movie M4, corresponding IR video for particle 1 at 480 K; Movie M5, particle 1 view at 580 K, particle gas release and ignition; Movie M6, corresponding IR video for particle 1 at 580 K; Movie M7, particle 2 view at 580 K, intense particle gas release and ignition; Movie M8, corresponding IR video for particle 2 at 580 K (ZIP)

■ AUTHOR INFORMATION

Corresponding Authors

Michelle L. Pantoya − *Department of Mechanical Engineering, Texas Tech University, Lubbock, Texas 79409-1021, United States;* ⓞ orcid.org/0000-0003-0299-1832; Email: michelle.pantoya@ttu.edu

Ralf I. Kaiser − *Department of Chemistry, University of Hawai'i at Manoa, Honolulu, Hawaii 96822, United States;* ⓞ orcid.org/0000-0002-7233-7206; Email: ralfk@hawaii.edu

Authors

Grace L. Rizzo − *Department of Chemistry, University of Hawai'i at Manoa, Honolulu, Hawaii 96822, United States*

Souvick Biswas − *Department of Chemistry, University of Hawai'i at Manoa, Honolulu, Hawaii 96822, United States*

Ivan Antonov − *Department of Chemistry, University of Hawai'i at Manoa, Honolulu, Hawaii 96822, United States*

Kelsea K. Miller − *Department of Mechanical Engineering, Texas Tech University, Lubbock, Texas 79409-1021, United States*

Complete contact information is available at:
https://pubs.acs.org/10.1021/acs.jpclett.3c00273

Author Contributions

G.L.R. designed and performed experiments, analyzed data, and prepared the manuscript. S.B. mentored G.L.R. and helped in experiments. I.A. wrote the Python script for analysis of kinetic data. K.K.M. and M.L.P. provided AIH and AID particles. All the authors contributed to reviewing and editing. R.I.K. designed, oversaw, and secured resources for the research project and supervised the manuscript preparation.

Notes

The authors declare no competing financial interest.

■ REFERENCES

(1) Faraday, M. Experimental Relations of Gold (and Other Metals) to Light. *Philos. Trans. R. Soc. London* **1857**, *147*, 145−181.

(2) Edwards, P. P.; Thomas, J. M. Gold in a Metallic Divided State-From Faraday to Present-Day Nanoscience. *Angew. Chem., Int. Ed.* **2007**, *46*, 5480−5486.

(3) Dreizin, E. L. Metal-Based Reactive Nanomaterials. *Prog. Energy Combust. Sci.* **2009**, *35*, 141−167.

(4) E, X. T. F.; Pan, L.; Wang, F.; Wang, L.; Zhang, X.; Zou, J. J. Al-Nanoparticle-Containing Nanofluid Fuel: Synthesis, Stability, Properties, and Propulsion Performance. *Ind. Eng. Chem. Res.* **2016**, *55*, 2738−2745.

(5) Lucas, M.; Brotton, S. J.; Min, A.; Pantoya, M. L.; Kaiser, R. I. Oxidation of Levitated exo-Tetrahydrodicyclopentadiene Droplets Doped with Aluminum Nanoparticles. *J. Phys. Chem. Lett.* **2019**, *10*, 5756−5763.

(6) Dikici, B.; Dean, S. W.; Pantoya, M. L.; Levitas, V. I.; Jouet, R. J. Influence of Aluminum Passivation on the Reaction Mechanism: Flame Propagation Studies. *Energy Fuels* **2009**, *23*, 4231−4235.

(7) Gesner, J.; Pantoya, M. L.; Levitas, V. I. Effect of Oxide Shell Growth on Nano-Aluminum Thermite Propagation Rates. *Combust. Flame* **2012**, *159*, 3448−3453.

(8) Trunov, M. A.; Umbrajkar, S. M.; Schoenitz, M.; Mang, J. T.; Dreizin, E. L. Oxidation and Melting of Aluminum Nanopowders. *J. Phys. Chem. B* **2006**, *110*, 13094−13099.

(9) Shancita, I.; Miller, K. K.; Silverstein, P. D.; Kalman, J.; Pantoya, M. L. Synthesis of Metal Iodates From an Energetic Salt. *RSC Adv.* **2020**, *10*, 14403−14409.

(10) Kalman, J.; Smith, D. K.; Miller, K. K.; Bhattacharia, S. K.; Bratton, K. R.; Pantoya, M. L. A Strategy for Increasing the Energy Release Rate of Aluminum by Replacing the Alumina Passivation Shell with Aluminum Iodate Hexahydrate (AIH). *Combust. Flame* **2019**, *205*, 327−335.

(11) Smith, D. K.; McCollum, J.; Pantoya, M. L. Effect of Environment on Iodine Oxidation State and Reactivity with Aluminum. *Phys. Chem. Chem. Phys.* **2016**, *18*, 11243−11250.

(12) Smith, D. K.; Bello, M. N.; Unruh, D. K.; Pantoya, M. L. Synthesis and Reactive Characterization of Aluminum Iodate Hexahydrate Crystals $[Al(H_2O)_6](IO_3)_3(HIO_3)_2$. *Combust. Flame* **2017**, *179*, 154−156.

(13) Gottfried, J. L.; Smith, D. K.; Wu, C. C.; Pantoya, M. L. Improving the Explosive Performance of Aluminum Nanoparticles with Aluminum Iodate Hexahydrate (AIH). *Sci. Rep* **2018**, *8*, 8036.

(14) Smith, D. K.; Unruh, D. K.; Wu, C. C.; Pantoya, M. L. Replacing the Al_2O_3 Shell on Al Particles with an Oxidizing Salt, Aluminum Iodate Hexahydrate. Part I: Reactivity. *J. Phys. Chem. C* **2017**, *121*, 23184−23191.

(15) Miller, K. K.; Gottfried, J. L.; Walck, S. D.; Pantoya, M. L.; Wu, C. C. Plasma Surface Treatment of Aluminum Nanoparticles for Energetic Material Applications. *Combust. Flame* **2019**, *206*, 211−213.

(16) Adams, D. M.; Hills, D. J. Single-Crystal Raman and Infrared Study of Aluminum Trichloride Hexahydrate. *J. Chem. Soc. Dalt. Trans.* **1978**, 782−788.

(17) Sherwood, P. M. A.; Turner, J. J. Vibrational Spectra of Compounds in the Iodine Pentoxide -Water System and Sodium Iodate. *Spectrochim. Acta A Mol. Biomol. Spectrosc.* **1970**, *26*, 1975−1992.

(18) Durig, J. R.; Bonner, O. D.; Breazeale, W. H. Raman Studies of Iodic Acid and Sodium Iodate. *J. Phys. Chem.* **1965**, *69*, 3886−3892.

(19) Degen, I. A.; Newman, G. A. Raman Spectra of Inorganic Ions. *Spectrochim. Acta A Mol. Biomol. Spectrosc.* **1993**, *49*, 859−887.

(20) Hibben, J. H. *The Raman Effect and Its Chemical Applications*; Reinhold Publishing Corp.: New York, NY, 1939.

(21) Ngo, N.; Kalachnikova, K.; Assefa, Z.; Haire, R. G.; Sykora, R. E. Synthesis and Structure of $In(IO_3)_3$ and Vibrational Spectroscopy of $M(IO_3)_3$ (M = Al, Ga, In). *J. Solid State Chem.* **2006**, *179*, 3824−3830.

(22) Bushiri, M. J.; Kochuthresia, T. C.; Vaidyan, V. K.; Gautier-Luneau, I. Raman Scattering Structural Studies of Nonlinear Optical $M(IO_3)_3$ (M = Fe, Ga, α-In) and Linear Optical β-$In(IO_3)_3$. *J. Nonlinear Opt. Phys. Mater.* **2014**, *23*, 1450039.

(23) Steinfeld, J. I.; Francisco, J. S.; Hase, W. L. *Chemical Kinetics and Dynamics*; Prentice Hall, Inc.: Upper Saddle River, NJ, 1999.

(24) Ellestad, O. H.; Woldbæk, T.; Kjekshus, A.; Klæboe, P.; Selte, K. Infrared and Raman Studies of Crystalline I_2O_5, $(IO)_2SO_4$, $(IO)_2SeO_4$ and I_2O_4. *Acta Chem. Scand. A* **1981**, *35a*, 155−164.

(25) Maneva, M.; Koleva, V. Thermal and Calorimetric Investigations of $M(IO_3)_2 \cdot H_2O$ and $M(IO_3)_2 \cdot D_2O$ (M^{2+}= Ca^{2+}, Sr^{2+}, Ba^{2+}). *Thermochim. Acta* **1992**, *207*, 85−93.

(26) Maneva, M.; Koleva, V. Thermal and Calorimetric Studies of $M(IO_3)_2 \cdot 6H_2O$ and $M(IO_3)_2 \cdot 6D_2O$ for M^{2+}= Ca^{2+} and Sr^{2+}. *J. Therm. Anal.* **1992**, *38*, 2491−2499.

(27) Koleva, V.; Maneva, M. Kinetic Analysis of the Dehydration Processes in Some Iodate Hydrates. *Thermochim. Acta* **1994**, *242*, 233−237.

(28) Rubtsov, N. M.; Tsvetkov, G. I.; Chernysh, V. I.; Troshin, K. Y. Features of Hydrogen and Deuterium Ignition Over Noble Metals at Low Pressures. *Combust. Flame* **2020**, *218*, 179−188.

(29) Tappan, B. C.; Dirmyer, M. R.; Risha, G. A. Evidence of a Kinetic Isotope Effect in Nanoaluminum and Water Combustion. *Angew. Chem., Int. Ed.* **2014**, *53*, 9218−9221.

(30) Shackelford, S. A.; Goshgarian, B. B.; Chapman, R. D.; Askins, R. R.; Flanigan, D. A.; Rogers, R. N. Deuterium Isotope Effects During HMX Combustion: Chemical Kinetic Burn Rate Control Mechanism Verified. *Propellants Explos. Pyrotech.* **1989**, *14*, 93−102.

(31) Scott Tonner, D.; Tholmann, D.; McMahon, T. B. Deuterium Isotope Effect on the Radiatively Induced Unimolecular Dissociation of Small Cluster Ions. *Chem. Phys. Lett.* **1995**, *233*, 324−330.

(32) Smith, D. K.; Unruh, D. K.; Pantoya, M. L. Replacing the Al_2O_3 Shell on Al Particles with an Oxidizing Salt, Aluminum Iodate Hexahydrate. Part II: Synthesis. *J. Phys. Chem. C* **2017**, *121*, 23192−23199.

(33) Miller, K. K.; Creegan, S. E.; Unruh, D. K.; Pantoya, J. D.; Hill, K. J.; Tran, Q.; Pantoya, M. L. Acid Base Synthesis of Aluminum Iodate Hexahydrate Powder as a Promising Propellant Oxidizer. *Chem. Eng. J.* **2023**, *453*, 139953.

(34) Antonov, I.; Chyba, A.; Perera, S. D.; Turner, A. M.; Pantoya, M. L.; Finn, M. T.; Epshteyn, A.; Kaiser, R. I. Discovery of Discrete Stages in the Oxidation of exo-Tetrahydrodicyclopentadiene (C$_{10}$H$_{16}$) Droplets Doped with Titanium-Aluminum-Boron Reactive Mixed-Metal Nanopowder. *J. Chem. Phys. Lett.* **2022**, *13*, 9777−9785.